View metadata, citation and similar papers at core.ac.uk
brought to you by CORE
provided by DigitalCommons@USU

In Situ Surface Voltage Measurements of Dielectrics Under Electron Beam Irradiation

Joshua L. Hodges, JR Dennison, Justin Dekany,
Gregory Wilson, Amberly Evans, and Alec M. Sim

***Abstract*— New instrumentation has been developed for non-contact, *in vacuo* measurements of the electron beam-induced surface voltage as a function of time and position for non-conductive spacecraft materials in a simulated space environment. Used in conjunction with the capabilities of an existing ultrahigh vacuum electron emission analysis chamber, the new instrumentation facilitates measurements of charge accumulation, bulk resistivity, effects of charge depletion and accumulation on yield measurements, electron induced electrostatic breakdown potentials, radiation induced conductivity effects, and the radial dispersion of surface voltage.**

The novel system uses two movable capacitive sensor electrodes that can be swept across the sample to measure surface charge distributions on samples, using a non-contact method that does not dissipate sample charge. Design details, calibration and characterization measurements of the system are presented, for a surface voltage range from <1 V to >30 kV, voltage resolution <1 V, and spatial resolution <1.5 mm. Extensive characterization tests with externally biased conductors were performed to calibrate the system and determine the instrument stability, sensitivity, accuracy, range, spatial resolution and temporal response.

Two types of measurements have been made on two prototypical polymeric spacecraft materials, low density polyethylene (LDPE) and polyimide (Kapton HN™) to illustrate the research capabilities of the new system. First, surface voltage measurements were made using a pulsed electron beam, while periodically measuring the surface voltage. Second, post charging measurements of the surface voltage were conducted, as deposited charge dissipated to a grounded substrate. Theoretical models for sample charging and discharge are outlined to predict the time, temperature, and electric field dependence of the sample net surface voltage. The good agreement between the fitting parameters of the model is discussed and the corresponding physical parameters determined from the literature and measurements by related techniques.

***Index Terms*—materials testing, space environment interactions, instrumentation, electromagnetic flux, electron flux, conductivity, electron emission**

Research was supported by funding from the NASA James Webb Space Telescope project at the Goddard Space Flight Center and support from the US Air Force through the PALACE Acquire Program.

Joshua Hodges is a ??? with the Mature and Proven Aircraft Division, Hill Air Force Base in Ogden, UT 84056 USA (e-mail: Joshua.Hodges@hill.af.mil. JR Dennison is a professor with the Materials Physics Group in the Physics Department at Utah State University in Logan, UT 84322 USA (e-mail: JR.Dennison@usu.edu). Justin Dekany, Gregory Wilson and Amberly Evans are students in the Materials Physics Group. Alec Sim is an Instructor in the Department of Physical Sciences at Irvine Valley College, Irvine CA 92618 USA (e-mail: ASim@ivc.edu).

NOMENCLATURE

CF	=	voltage conversion factor
C_f	=	voltage sensor plate capacitance
C_s	=	sample capacitance
C_w	=	capacitance of EFTP wire and feedthrough
C_{WP}	=	witness plate capacitance
R_i	=	effective resistance to ground of EFTP
V_{offset}	=	probe offset voltage
V_p	=	measured electrostatic field probe voltage
V_s	=	sample voltage
(V_{drifto}/τ_D)	=	probe voltage drift rate
Δt	=	elapsed time since EFTP calibration to ground
ε_r	=	relative dielectric constant
ρ	=	resistivity
σ_s	=	sample charge density
σ_w	=	witness plate charge density
τ	=	probe voltage RC decay time
τ_D	=	thin film sample charge decay time

I. INTRODUCTION

Surface charging and subsequent electrostatic discharge due to interactions with the space environment is one of the primary concerns of spacecraft charging studies [A,B,C,1]. Laboratory measurements of the evolution of surface voltages and dissipation currents under simulated space conditions are the primary method used to determine the response of key materials to various incident fluxes.

The conductivity of the material is a key transport parameter in determining how deposited charge will distribute across the spacecraft, how rapidly charge imbalances will dissipate, and what equilibrium potential will be established under given environmental conditions [11,D]. The low charge mobility of insulators causes charge to accumulate where deposited, preventing even redistribution of charge and creating inhomogeneous local electric fields and potentials across the material. Hence, it is critical for reliable spacecraft charging models to use appropriate values of conductivity for thin film insulators to determine the correct charge distributions and charge storage decay times for the materials.

The bulk conductivity values of commonly used insulators have most often been found using standard ASTM prescribed methods [E], utilizing a parallel plate capacitor geometry and an voltage applied with electrodes (see Figure 1(a)). Similar tests have been done under vacuum conditions and more realistic space environments [F], but these methods, in some cases are not strictly applicable to situations encountered in

spacecraft charging [15,11,G]. Charge decay methods expose one side of the insulator in vacuum to sequences of incident charged particles, light or plasma, with a conductive electrode attached to the other side of the insulator. Data are obtained by capacitive coupling to measure both the resulting voltage on the open surface and emission of electrons from the exposed surface, as well monitoring both conductive and displacement currents to the electrode (Figure 1(b)).

This paper describes the design, construction, calibration, and testing of a system to measure the surface charge on an insulator as a function of time and position *in situ* in a spacecraft charging vacuum test chamber. Surface charge is generated by incident fluxes that deposit charge and energy near the surface, and create secondary and backscattered electrons which are emitted from the material. Deposited charge dissipates on relatively long time scales by charge transport through highly resistive materials to grounded substrates.

The general design parameters of the system are set by the extent of the spacecraft charging problem [H]. A desired lower voltage range and voltage resolution is 1 V, estimated as ~10% of the electrostatic breakdown potential for thin film sample such as oxide layers or dielectric coating on the order of 10^{-6} to 10^{-5} m with typical electrostatic field strengths of 10^{7} to 10^{8} V/m and breakdown voltages of 10^{1} to 10^{3} V. A desired upper voltage range is 30 kV, which is the upper bound on incident electrons that most affect surface charging events [I] and is also an upper bound on surface charging beyond which electrons penetrate far enough into materials that electron emission is minimal [J] and a typical breakdown voltage for common 100 µm thick blanket materials. Desired instrument response times can be estimated from dissipation times for low conductivity materials (10^{-12} $(\Omega\text{-cm})^{-1}$ to 10^{-20} $(\Omega\text{-cm})^{-1}$)—with corresponding dissipation times of a few times 10^{-1} s to 10^{7} s—identified as problematic in spacecraft charging [K]; this suggests a response time on the order of 1 s is appropriate and a system stable over a few days would be required to see a few percent decay in the lowest conductivity materials [H]. Spatial resolution on the order of a few mm is also desirable.

A detailed description of the instrumentation, including the surface voltage probe (SVP) and electrostatic field transfer probe (EFTP), are provided. We emphasize how the sensor is incorporated into the existing detector. We also describe measurements to characterize the stability, sensitivity, accuracy, range, spatial resolution and temporal response of the surface charge measurable by our system. A more extensive description is found in Hodges [H].

Two measurements are also described to illustrate the research capabilities of the test system. Surface voltage measurements were made periodically during the electron beam charging process and as the surface voltage discharged to a grounded substrate after exposure. Analysis of the measured curves provides information on the material electron yields and bulk resistivity. The evolution of the spatial profile of the voltage across the sample surface was also measured by sweeping a small electrode across the surface.

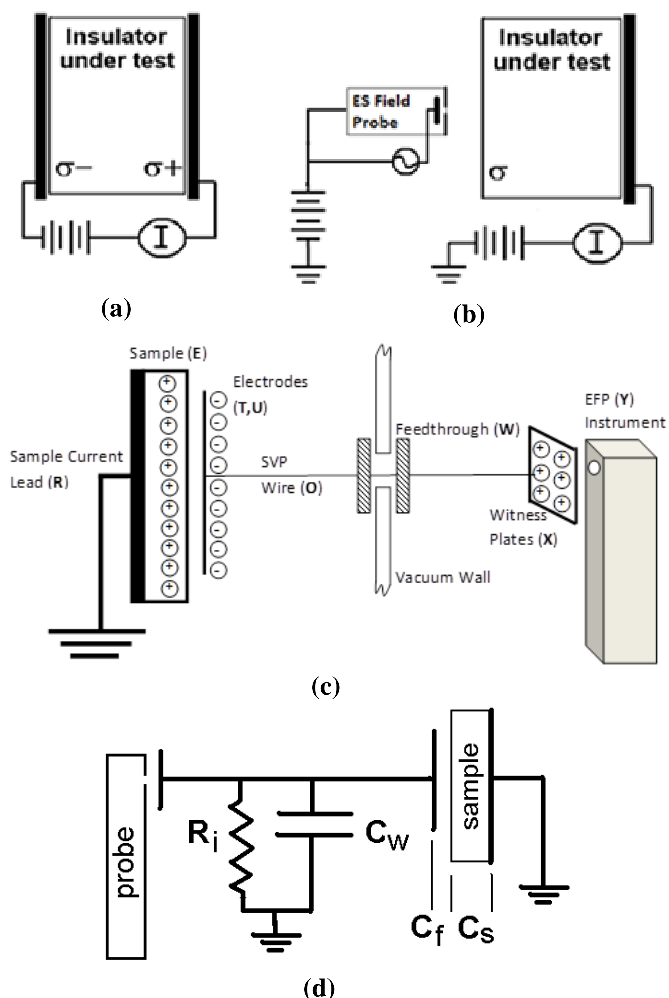

Fig. 1. Schematics of the EFTP assembly. *Schematic representation for two different resistivity measurements:* (a) *classical method and* (b) *charge storage method.* (c) *Charge distribution for the EFTP assembly. Shown are the sample (left), EFTP (center), and electrostatic field probe, (right). (d) Effective circuit for EFTP.*

II. INSTRUMENTATION

Our novel surface voltage probe system is shown below to meet the general design guidelines for measurements most relevant to spacecraft charging issues. The response time of the probe and data acquisition system are fast enough to acquire data for lower resistivity materials such as low density polyethylene (LDPE), with a few seconds decay times. The long term stability and drift characterization required to measure at slow rates and take data over several days on materials that have a high resistivity like Kapton necessitate computer controlled data acquisition.

Design details, calibration and characterization measurements of the system are presented, for a surface voltage range from <1 V to >30 kV, voltage resolution 1 V, and spatial resolution 1.5 mm. The novel system uses two movable capacitive sensor electrodes (3 mm and 7 mm diameter) that can be swept across the sample using an *in vacuo* stepper motor to measure surface charge distributions on samples *in situ*, using a non-contact electrostatic field probe method that does not dissipate sample charge.

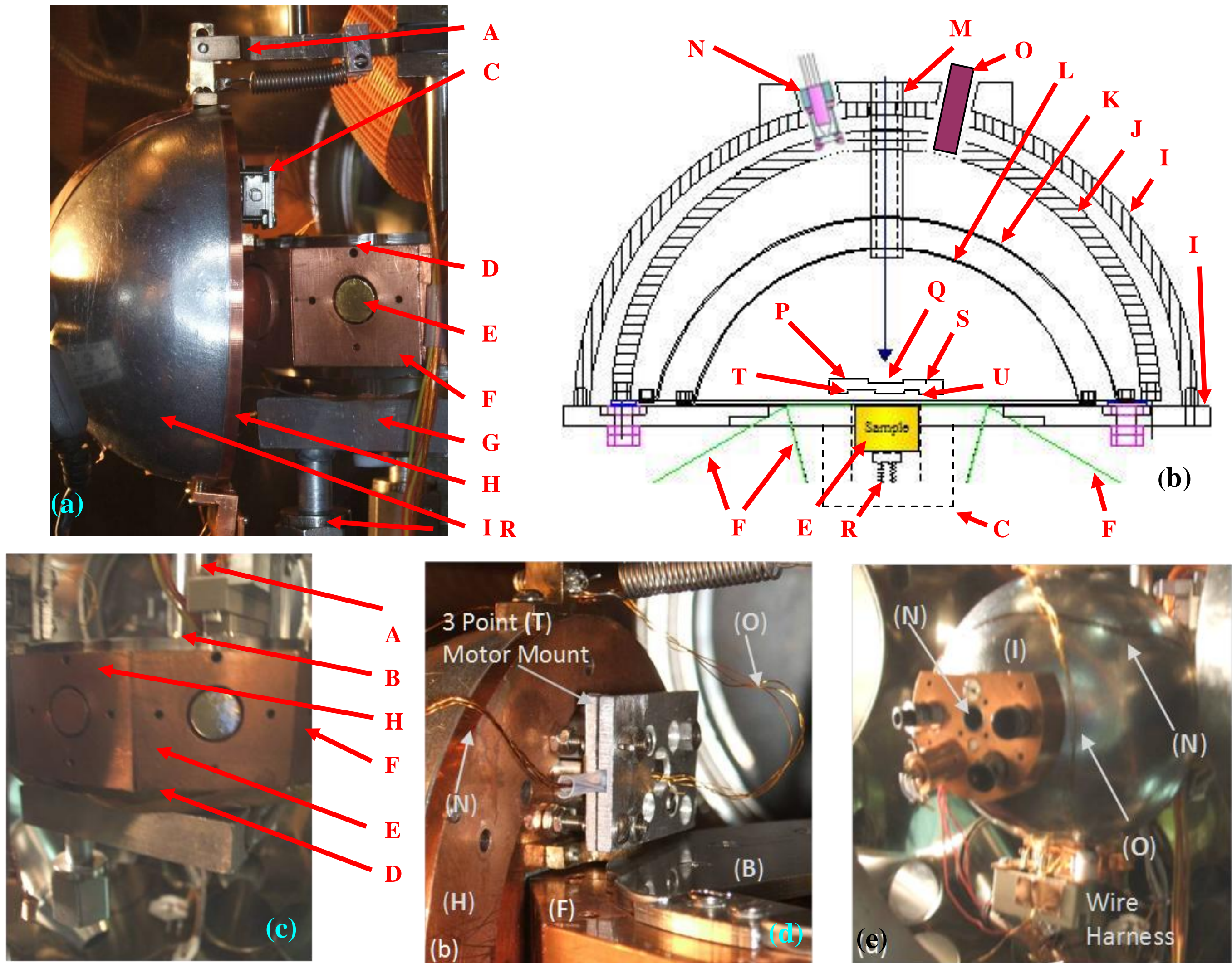

Figure 2. Hemispherical Grid Retarding Field Analyzer (HGRFA). *(a) Photograph of sample stage and HGRFA detector (side view). (b) Cross section of HGRFA. (c) Photograph of sample stage showing sample and cooling reservoir. (d) Side view of the mounting of the stepper motor. (e) Isometeric view of the HGRFA detailing the flood gun, optical ports, and wire harness.*

LEGEND

A *HGRFA Hinged Mount*	***I*** *HGRFA Hemispherical Shield*	***R*** *Sample Current Lead*
B *Sample Carousel/HGRFA Rotation Shaft*	***J*** *HGRFA Collector*	***S*** *SVP Faraday Cup*
	K *HGRFA Bias Grid*	***T*** *SVP 7 mm Diameter Au Electrode*
C *UHV Stepper Motor*	***L*** *HGRFA Inner Grid*	***U*** *SVP 3 mm Diameter Au Electrode*
D *Sample Block Faraday Cup*	***M*** *HGRFA Drift Tube*	***V*** *SVP Wiring Channel*
E *Sample (10 mm)*	***N*** *Electron Flood Gun*	***W*** *EFTP Vacuum Feedthrough*
F *Sample Block*	***O*** *LED Light Source*	***X*** *EFTP Witness Plate*
G *Cryogen Reservoir*	***P*** *Surface Voltage Probe (SVP)*	***Y*** *Electrostatic Field Probe*
H *HGRFA Face Plate*	***Q*** *Au Electron Emission Standard*	***Z*** *Probe XYZ Translator*

A. *Overview of Electron Emission Test Chamber*

The compact transfer probe design extends our measurement capabilities by allowing the surface voltage probe to fit within an existing hemispherical grid retarding field analyzer, so that surface voltages can be measured on samples tested using the extensive source flux and emission detection capabilities of the spacecraft charging vacuum test chamber. An overview of the main electron emission chamber is included to illustrate the full capabilities of the surface voltage test system.

The primary instrument of the Utah State University (USU) test facility to study electron emission from conductors and insulators is a versatile ultra-high vacuum (UHV) chamber with surface analysis and sample characterization capabilities. This system is described in more detail elsewhere.[1-7] This chamber can simulate diverse space environments including controllable vacuum ($<10^{-10}$ to 10^{-3} Torr) and ambient neutral gases conditions, temperature (<40 to >400 K), as well as sources for a broad range of electron, ion and photon fluxes

and energies. A variety of detectors are available for measurements of single or simultaneous electron-, ion-, and photon-induced emission,[2,4,5] including a standard Faraday cup detector, hemispherical analyzer, cylindrical mirror, and time of flight micro-channel plate detector. Specifically, they allow us to measure total emitted electron (ion) yield, backscattered/secondary yield, charge decay curves, and energy spectra.[1]

Two primary electron sources provide monoenergetic electron beams ($\Delta E/E<2\cdot10^{-4}$) with electron energy ranges from ~20 eV to ~30 keV and incident electron currents ranging from 0.1 nA to 10 μA, beam spot FWHM diameters ranging from ~50 μm to >100 mm (depending on beam energy), and pulsing capabilities ranging from 10 ns to continuous emission. The low energy electron gun (Staib, Model NEK-050-SP) with a W filament is operated at incident electron energies of ~20 eV to 5000 eV with a typical beam current of ~ 10 nA and a typical ~3 mm FWHM diameter beam spot. The high energy electron gun (Kimball, Model EGPS-21B) using a LaB_6 emitter is operated at incident electron energies of 5 keV to 25 keV with a typical beam current of ~20 nA and a typical 500 μm diameter beam spot. Stable, uniform, well-characterized beam fluxes of 0.05 nA-cm^{-2} to >1 μA-cm^{-2} are possible from the electron guns. There are also three ion guns with <0.1 to 5 keV monoenergetic sources for inert and reactive gases; one (PHI, Model I11-065) has rastering and pulsed deflection capabilities. The NIR-VIS-UV solar irradiance spectrum is simulated using a pair of pulsed, monochromated lamp sources: (i) a Tungsten/halogen lamp system with a Suprasil envelope produces focused (~0.5 cm diameter) radiation from 0.4 eV to 7.2 eV (200 nm to 2000 nm) and (ii) a deuterium RF powered continuum source with a MgF_2 window produces focused (~0.5 cm diameter) radiation from 3.1 eV to 11.1 eV (150 nm to 400 nm). Additional light sources include a Kr resonance lamp (10.3 eV), broadband Hg discharge and W-filament sources, and a variety of quasi-monochromatic NIR/VIS/UVA LED sources.[1]

For conducting samples, electron guns are operated using a continuous, low-current beam of electrons, and dc-currents are measured with standard ammeters sensitive to $.10^{-13}$ A. The system at USU to measure electron emission from insulators uses a combination of methods to control the deposition and neutralization of charge. Typically, charge deposition is minimized by using a low current beam (~10-30 nA) focused on a sample area of ~7 mm^2 that is delivered in short pulses of ~5 μsec. Each pulse contains ~150 fC or ~10^5 electrons-mm-2. For a typical ~100 μm thick dielectric sample, this amount of charge is estimated to change the surface potential by only 10-100 mV/pulse (positive) and requires ~500 pulses/sec to achieve an ~1 nA/cm^2 dosage that typically causes discharge in space. The pulsed system uses custom detection electronics developed at USU with fast (1-2 μs rise time) sensitive/low noise (10^7 V/A / 100 pA noise level) ammeters for determining insulator emission with minimal charging effects.[4,5] Detected current pulses from the ammeters are sent to a fast (100 MHz, 1 GS/s) digital storage oscilloscope (Tektronics Model TDS 2014). Charge dissipation techniques include a custom low energy (~1-10 eV) electron flood gun for direct neutralization of positively charged surfaces between incident pulses.[4,5,8] A variety of visible and UV light sources are used for neutralization of negatively charged surfaces through the photoelectric effect. Sample heating to ~50-100 °C has also been used for dissipation of buried charge by thermally increasing the sample conductivity. Often, samples will be heated to ~50 °C over night to increase conductivity and dissipate charge after a day of electron emission measurements. Both DC and pulsed measurements and data retrieval are fully computer automated, using GPIB interfacing and a DAQ card under LabVIEW™ control. A complete description of the DC-system and pulsed-system setups, along with additional insulator-yield and charging data, is available in other references.[2-5]

B. Detector Assembly

The primary detector for emission studies is a custom hemispherical grid retarding field analyzer (HGRFA), with a retarding-field analyzer grid system for emitted-electron energy discrimination between back scattered electrons (energies >50 eV) and secondary electrons (energies <50 eV) (see Fig. 2). By ramping the grid (refer to labels **K** and **L** in Figure 2) bias, energy spectra of the emitted electrons can also be measured using this detector. The HGRFA features an aperture and drift tube (**M**) for incident electron/ion admission and a fully-encasing hemispherical collector (**J**) for full capture of emitted electrons, that is particularly well suited and calibrated for absolute yield measurements.[2,3,5] The hemispherical grid detection system has been carefully calibrated (both through calculation and measurement) to account for detector losses, allowing yield accuracies of better than 2% for conductor yields and better than 5% for insulator yields.[1,2] The HGRFA can be independently positioned in front of any sample (**E**) (see Fig. 2(a)). A low energy flood gun (**N**) and a variety of visible and UV LED light sources (**O**) are mounted on the HGFRA housing at near-normal incidence to provide neutralization of surface charging between pulses. A collimating lens mounted on the HRFA and attached to a fiber optic cable and vacuum feedthrough allow external light sources to be used or a photospectrometer to analyze emitted light from the sample. The flood gun (**N**) also acts as a low energy (~1eV to 100 eV) focused electron source.

C. Sample Assembly

Samples (**E**) are mounted on (10.0 ± 0.1) mm diameter Cu cylinders, usually using a Cu tape with conductive, UHV-compatible adhesive routinely used for scanning electron microscope studies (3M, Type 1182 tape) or with UHV compatible, low-temperature, conductive epoxy (Masterbond, EP21TDCS-LO). Sample up to 26 mm in diameter can be accommodated in the sample mounts. The Cu cylinders are mounted in sample blocks (**F**) on the sample carousel, using ceramic pins or 100 μm diameter sapphire spheres held in place with set screws to provide electrical isolation. Electrical connection to the sample is made via one or more spring loaded pins (**R**) from the rear, allowing the current(s) to the sample to be monitored. The primary sample carousel is a right dodecagon that has eleven sample blocks that can be rotated in front of the various flux sources (see Fig. 2(c)). Typically, one sample block contains a photodiode, another a Faraday cup, and a third a Au sample as an electron emission standard (see Fig. 2(e)). The sample carousel can be easily removed for rapid sample exchange. The samples are positioned mechanically via a grooved plate that locates the

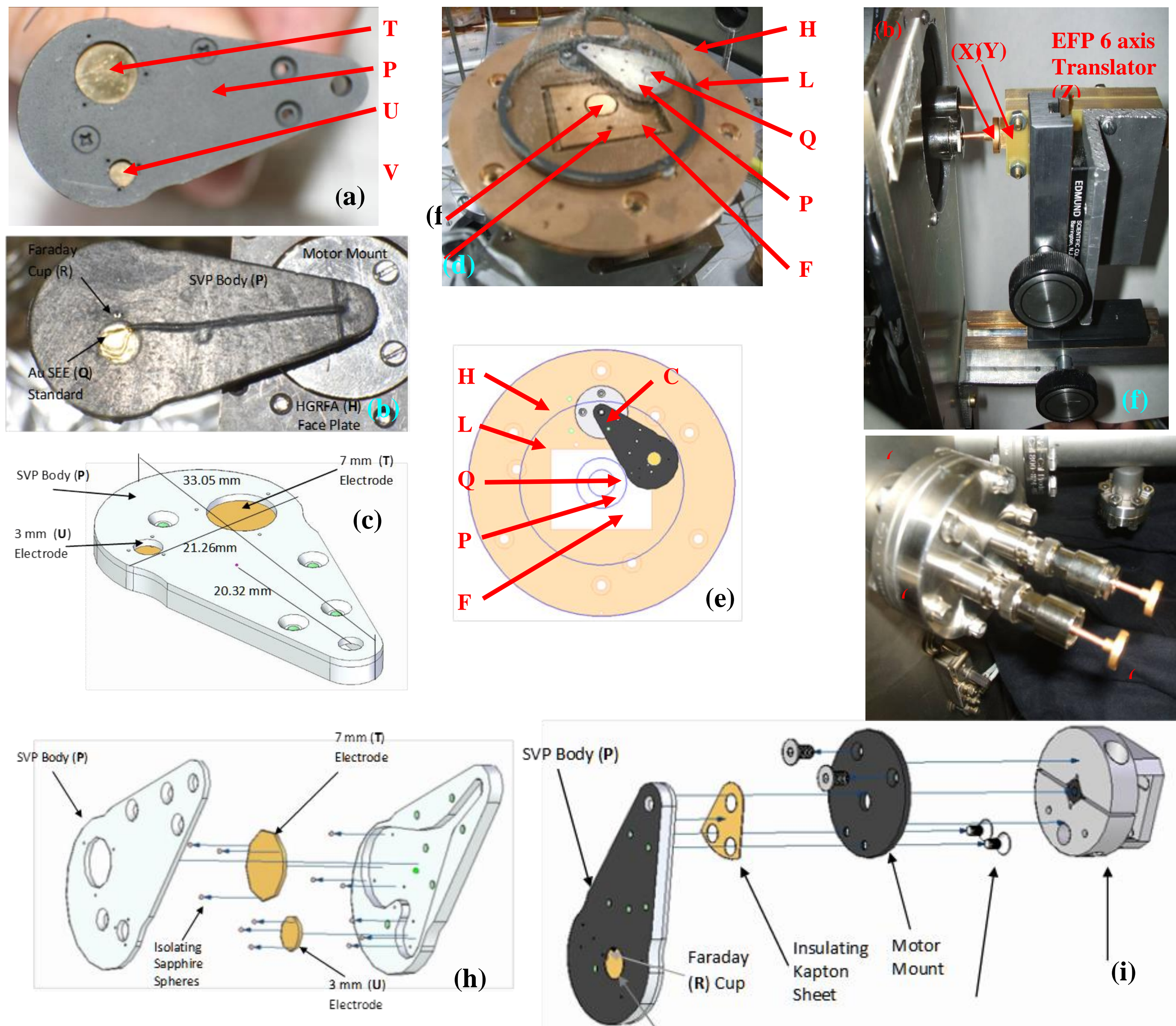

Fig. 3. Surface Voltage Probe (SVP). *(a) Photograph of sample side of surface voltage probe assembly. (b) Photograph of Au SEE standard and Aquadag surface of the SVP. (c) Overall dimensions of SVP with center of gravity indicated. (d) Photograph of the SVP ,omyrd on the HGRFA, with the collecting hemisphere removed. (e) Diagram of HGRFA interior with SVP, looking toward the sample. (f) 6 axis EFP translation stage mounted parallel to a witness plate. (g) Air side of SVP with witness plate feedthrough and connectors. (h) Exploded view of SVP internal parts. (i) Exploded view of SVP motor assembly.*

HGRFA face plate with an accuracy of ±0.5 mm from the sample. *Ex situ* tests have shown that there is no significant degradation in the calibration factors for changes in probe to sample distances <5 mm.

The sample carousel is mounted on a cryogenic reservoir (Fig. 2(d)); it is electrically isolated using a ~75 µm thick Cotherm™ sheet that provides good thermal contact. Liquid nitrogen cooling allows samples to achieve temperatures of ~115 K within 4 hrs, using a temperature controller (Omega, Part #CNi16D33-EI) connected to a liquid nitrogen solenoid to maintain the sample temperature to within ±5K. Temperatures 400 K can be achieved using a resistive heating element (Omega CSS-01115/120V) that are controlled (Omega CN9000A PID controller) to within ± 1 K. The large thermal mass of the sample stage help minimize temperature fluctuations.

An alternative low-temperature sample stage has been developed for use with the HGRFA/SVP assembly [L]. The sample holder uses a closed cycle He cryostat to attain sample temperatures from 40 K to >350 K, with 0.5 K stability maintained by a standard PID temperature controller (RMS Technologies, Model ???) using platinum resistance thermometers and resistive heaters.

D. Surface Voltage Probe Design

The surface voltage probe (SVP) is a small device that fits within the HGRFA to measure the surface potential of a sample. Figure 4 shows a block diagram of the SVP system and electronics. Figure 3(c) shows the assembled SVP, which is <40 mm long and only ~21 mm wide, with a thickness of <3 mm. Two openings in the casing of 7.0 mm (**T**) and 3.0 mm (**U**) diameter define the effective electrode areas. The casing is coated with colloidal graphite to minimize the production of

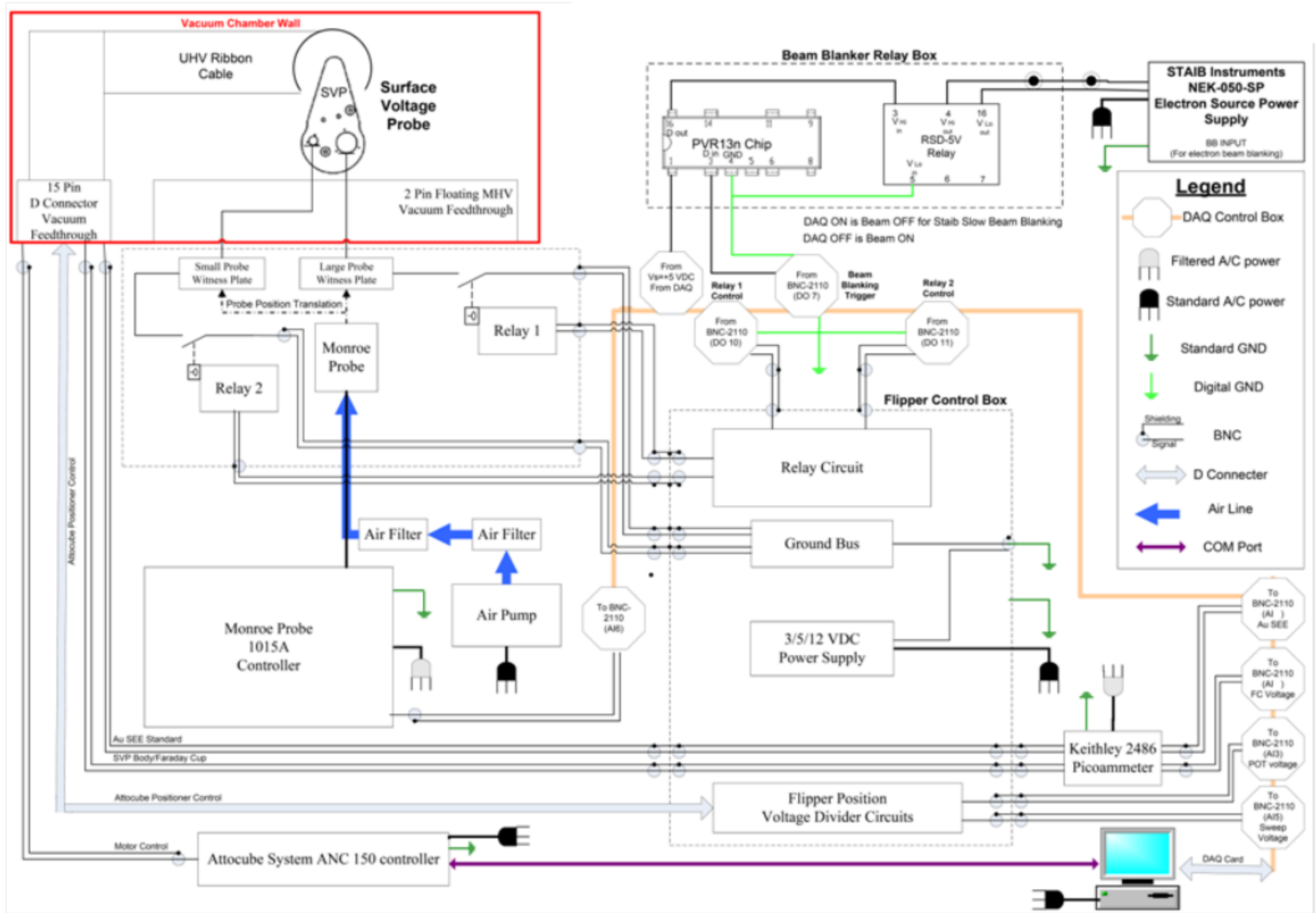

Fig. 4. Surface Voltage Probe block diagram.

secondary electrons by stray electrons inside the HGRFA (see Figs. 3(a) and 3(b)). There are two electrodes (**U** and **T**) on the sample side of the sensor ~500 µm above the sample surface, each kinematically positioned by six 76 µm diameter sapphire spheres above and below the electrodes. The electrodes are very well electrically isolated from the outer casing of the unit by the sapphire spheres. The electrodes are Au plated to minimize surface contamination and allow a uniform charge density on the probe. Currents to the two electrodes, the Au disc, and the full SVP casing can be monitored independently because each are electrically isolated. The two voltage sensor plates are each connected separately to external witness plates (**X**).

The SVP is mounted on a small sized (~25 mm x 11 mm diameter), ultra-high vacuum-compatible stepper motor (Attocube Systems, Model ANR50res) (**C**). The microstepper controller (Model ANC200), with a resistive position encoder, provides rapid and extremely fine (<1 m° per step) positioning. The SVP can be positioned on either side of the sample providing an unobscured view for the incident beam and can be swept from side to side allowing either electrode to pass fully over the sample.

The EFTP is a much smaller detector than commercial electrostatic field probes; this allows the SVP to be incorporated within the HGRFA (see Figs. 3(d) and 3(e)). Positioning the SVP inside the HGRFA has several advantages. The primary advantage is that surface voltage measurements can be made rapidly, while the sample and HGRFA are accurately aligned with the incident beam. In addition, an electrically isolated 4.15 mm diameter Au disc (**O**) is mounted on the source side of the probe and can be swung into place above the sample in line with an incident beam, providing a Au electron emission calibration standard for the detector [M,N,O]. Further, the SVP in this position can act as a shield for the sample preventing any stray electrons or light from charging or discharging the sample. There is also a 360 µm diameter Faraday cup (**S**) in the source side of the probe that can be swept across the sample to center the beam on the sample.

E. Electrostatic Field Transfer Probe Design

The EFTP used here is based on Frederickson's idea that a transfer probe can induce a surface voltage on an external witness plate proportional sample surface voltage, that can be easily measurable outside of the vacuum.[11,13] The EFTP (see Figs. 3 (f) and 3(g)) consists of a surface voltage probe electrodes (**U** or **T**) positioned above the sample (one of the) connected to an external witness plate (**X**) by ~1 m of thin 152 µm diameter 36AWG manganin wire (Lakeshore, Part # WSL-32-100) with very thin polyvinyl formal (Formvar®) insulation to minimize the capacitance of the EFTP. Each electrode is each connected to a 4 mm x 15 mm diameter polished Au-plated external witness plate (**X**) mounted on an ultrahigh high vacuum compatible dual floating MHV feedthrough (MDC Vacuum, Model MHV-275-2) (**W**) positioned outside the vacuum chamber close to a standard

electrostatic field probe (**Y**) (see Fig. 3(g)). The sensor of the electrostatic field probe (Monroe Electronics Isoprobe, Model 162) (**Y**) is mounted on a precision XYZ translation stage (**Z**) to precisely position the probe in front of one or the other witness plates with a ~500 µm probe-to-plate separation. The electrostatic field probe control electronics (Monroe Electronics, Model 1017AEL) can measure surface voltage of ±10 V with a resolution of ±1 mV. Provisions have been made to alternately mount another electrostatic field probe (Trek, Model 341 A) that can measure surface voltages of ±20 kV with ~0.5 V resolution to measure higher sample voltages. The probes and witness plates are mounted in a metal enclosure that provides electrostatic shielding and allows purging of the enclosure with dry nitrogen to reduce leakage voltages across the plate gaps due to moist air.

There are distinct advantages in using the EFTP and having the electrostatic field probe outside the vacuum chamber. Others have measured the surface voltage directly with electrostatic field probes inside the vacuum chamber and adjacent to the sample;[14,15] however, these methods were often subject to problems.[9,10] The required proximity of the electrostatic probe to the sample means that stray electron beam radiation—from secondary scattering, insufficient beam columniation, or beam rastering—can charge the sensitive electrostatic probe, often driving it off scale. Because it is difficult to discharge a probe in the vacuum, this can lead to large, unpredictable and persistent voltage offsets and can even damage the probe that cannot be readily repaired *in vacuo*.

III. CALIBRATION AND MEASURMENTS

A. Measurement Principles

To accurately measure a surface voltage with the EFTP, the sample plate and witness plate are positioned adjacent to grounded surfaces and the EFTP is grounded. This assures that there is no net charge on the EFTP and that the charge density is zero on both plates. The EFTP is then disconnected from ground and the witness plate voltage is measured with the electrostatic field probe; this provides a measure of the zero offset V_{offset}, that is the measured probe voltage for a grounded sample. A known voltage is then placed on a conducting sample. This causes an equal magnitude and opposite polarity charge density to form on the voltage sensor plate. However, since there is still no net charge on the EFTP (assuming that the probe is fully isolated), an equal magnitude charge is found at the opposite end of the EFTP. The charge density on the witness plate, σ_w, is then of the same polarity as the sample charge density, σ_s, with magnitude of the witness plate charge density scaled by the ratio of the voltage sensor plate capacitance to witness plate capacitance, $\sigma_w=(C_f/C_{WP})\sigma_s\equiv CF\bullet\sigma_s$. The proportionality constant, CF, depends on the plate areas and separations, but can be determined directly by measuring the witness plate voltage with the external electrostatic field probe for a variety of applied sample voltages. Figure 5(a) shows such a calibration curve for the large electrode. Once calibrated, the EFTP can then be used to measure unknown surface voltages or charge densities of conducting or insulating samples.

In an ideal system, the probe has infinite resistance and zero capacitance coupling to ground. More correctly, one must

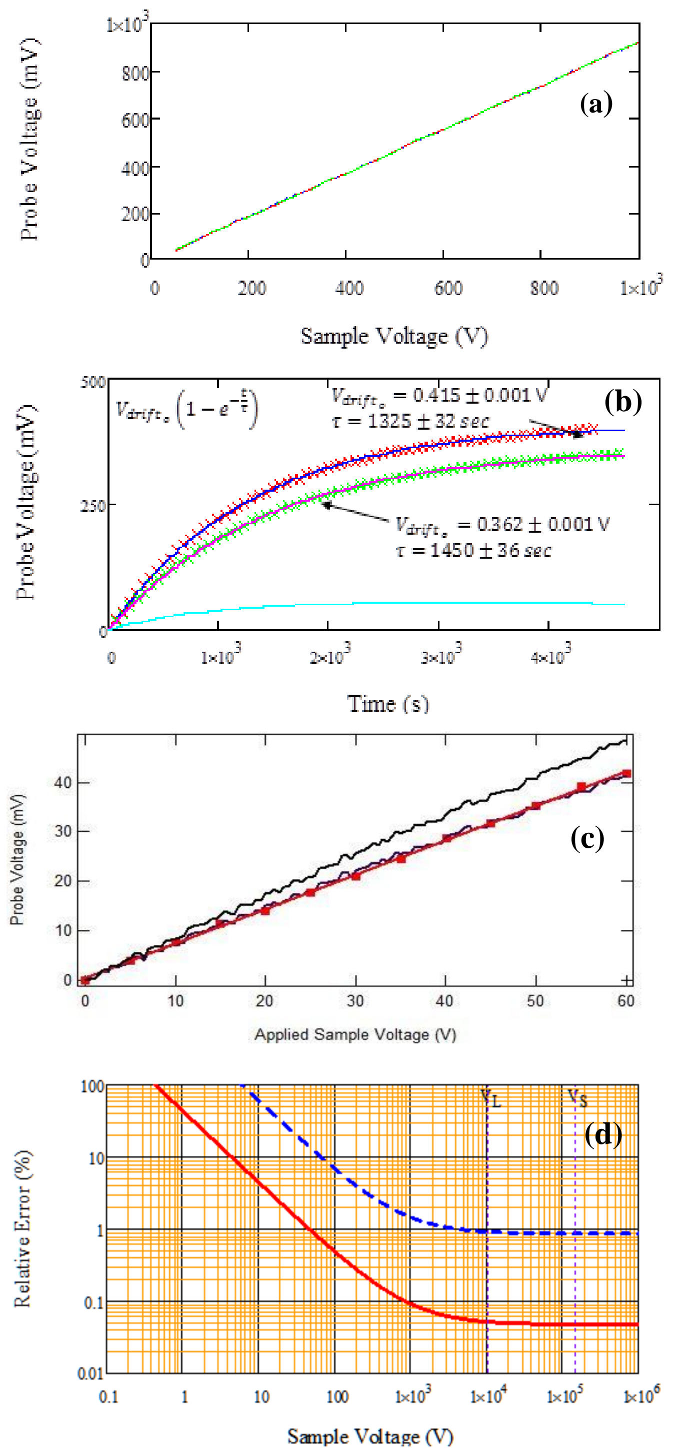

Fig. 5. Surface Voltage Probe (SVP) calibration tests. (a) Three super imposed calibration curves of the large electrode. (b) Graph of *in situ* measurements and exponential fits of the drift of the SVP over ground, with an average slope (V_{drifto}/τ_D)=280 µV_p/s at early times. Cyan curve shows the difference in the exponential fits. (c) Voltage calibration of probe voltage to an applied sample voltage. Red symbols are for data taken at 5 V and ~3 s intervals over ~1 min. The black curve is for data measured at 0.5 V and ~6 s interval over ~12 min. The blue curve shows data from the black curve after a linear correction for voltage drift. The red curve is a linear fit to the corrected data with a slope of (666±4) µV_p/V_s and an intercept of (3.5±0.5) µV_p. (d) Graph of relative error as a function of surface voltage. Large electrode (Red) and the small electrode (Blue), vertical red lines show the voltage limits of the large probe where the vertical blue lines show the voltage limit of the small probe.

consider the coupling of the EFTP to ground, including both the capacitance of the wire and probes and the leakage resistance to ground through the feedthrough, wire insulation, and probe mounts.[9] Figure 2(d) shows an equivalent circuit, where C_w is the wire and feethrough capacitance, R_i is the leakage resistance of the EFTP, and C_f is the capacitance of the sample surface to the voltage sensor plate. For a voltage on the sample, V_s (or equivalently a charge $Q_s=C_s \bullet V_s$, where C_s is the capacitance of the sample surface to both the voltage sensor plate and ground), the electrostatic field probe will read a voltage

$$V_s = \left(\frac{C_W + C_f}{C_f} \right) V_{p_o} e^{-t/\tau} \qquad with \quad \tau = R_i C_W \qquad (1)$$

The initial probe voltage V_{po} decays with time as charge leaks into (or from) the EFTP, with an RC time constant, τ. The value of R_i is actually only an effective resistance, since decay occurring initially is primarily a result a displacement current due to the capacitor polarization and only later due to a resistive current due to charge leakage. The three largest sources of a resistance are the leakage through air of the witness plate to the EFTP ($\sim 4 \cdot 10^{14}$ Ω), the electrical isolation of the electrodes to the probe body through the sapphire spheres ($\sim 3 \cdot 10^{14}$ Ω), and the vacuum feedthrough to ground ($\sim 1 \cdot 10^{14}$ Ω). The highest sources of capacitance of the probe are the capacitance of the feedthrough (~12 pF) and the capacitance of the wire (~6 pF).

Another reason for preferring the EFTP arrangement relates to electron emission from insulators.[11] Electron beam charging of the samples produces an electric field at the surface of the sample that can drive electrons out of the surface. While penetrating into the insulator, the high-energy electrons excite electrons and holes into trapping states and into mobile states located in the region between the sample surface and the maximum depth of penetration. Such trapped charge provides the charge to be later emitted from the surface. This effect is sometimes termed the Malter effect [P,?]. An *in situ* electrostatic field probe can collect these delayed emitted electrons, thereby altering the net charge on the electrostatic field probe and modifying the voltage reading with time.

The same modification of the net charge on the EFTP can occur for *ex situ* electrostatic field probes. However, by knowing the capacitance, C_f, the rate of voltage change on the voltage sensor plate provides a direct, sensitive method to determine the electron currents leaving the sample surface. After establishing V_{offset} when the sensor field plate faces ground (where no Malter emission occurs), the sample is rotated before the sensor and held there for a period of time, t. The measured voltage will change both because current is emitted from the sample to the sensor field plate and because the sample voltage is decaying. After the sensor field plate has collected charge, it is again faced to ground and its new V_{offset} reading shows how much charge was absorbed during time t. Measurements of the decay of surface voltage, performed rapidly so that negligible charge is delivered from the sample to the sensor plate, provides independent information about the total loss of charge from the sample. Subtracting the emitted charge from the total charge loss provides the charge conducted through the sample to the grounded electrode, which can in principle be measured directly by the electrometer attached to the grounded electrode for direct comparison (at least for relatively large leakage rates).

B. Calibration

To determine the calibration factor of the EFTP, measurements were made of the probe voltage for a series of known sample voltages, as shown in Figure 5(a). The large electrode has a repeatable calibration factor of CF=1084.5±0.5 V_p/V_s over a range of applied voltages >1000 V. It is good practice to determine the calibration factor for each set of experiments as well, as there is some small variation due to specific sample and sensor conditions and separation. Tests also indicated that an accurate surface voltage measurement could be made in <500 ms, as limited by the time constant of the EFTP (~100 ms), the response time of electrostatic field probe (<5 ms), and data acquisition time.

The probe offset voltage (typically on the order of a few mV) and voltage drift with time were found to differ for each test and must be measured for each test sequence by performing an applied voltage calibration run. To calibrate the EFTP drift due to leakage, a constant voltage was placed on the sample and the probe voltage was monitored with time over ~2 hr, as shown in Figure 5(b). The voltage was found to change almost linearly with time over early times at a rate of (V_{drifto}/τ_D)=280 μV/s. Measurements made for nonzero applied voltages produced very similar drift rates. Without correcting for voltage drift, there would be a ~0.5 V error in measured surface voltage, comparable to the instrument resolution, in ~12 s. After correcting for a linear drift, measurements can be taken for > 4 hr with <20 V error.

Drift correction is further illustrated in Fig. 5(c). An initial set of surface voltages were taken rapidly at 5 V and ~3 s intervals over ~1 min. These data exhibited a highly linear dependence with a calibration factor of CF=(1.502±0.009) $V_s/\mu V_p$ and an offset voltage of V_{offset}=(3.5±0.5) μV_p. A second set of data were taken more slowly at 0.5 V and ~6 s interval over ~12 min. These data had a somewhat larger slope due to voltage drift. However, when corrected for a linear drift, the longer duration data set agreed very well with the shorter duration data set. Measurements of a grounded sample voltage were stable over hours to ~0.1 V after correcting for a linear voltage drift and initial V_{offset}.

Hodges provides a much more detailed discussion of the calibration that becomes relevant for operation of the SVP requiring higher precision or longer times between recalibration [H]. His calibration extends the linear approximation for drift in Eq. 2 to an exponential correction as expressed in Eq. 1 and additional corrections for the drift in the detector electronics and exponential drifts in time and voltage of the sample voltage.

Combining the results of the calibration tests, the measured probe voltage is related to the actual surface voltage through a linear approximation to Eq. 1 as:

– - - —— - (2)

where $(t\text{-}t_d)$ and $(t\text{-}t_v)$ are the elapsed time since recalibration of the probe to a grounded surface and the that the probe has been positioned over a sample, respectively. For times 150 s voltage drift is negligible (*i.e.*, $\beta \rightarrow 0$) and a linear approximation for the temporal drift introduced errors less than other sources of error. The EFTP and SVP assembly was

sensitive to a surface voltage of <1 V with a resolution of ~0.5 V. Surface voltages up to ±12 kV could be measured with the Monroe probe. Much higher voltages (in principle up to ±20 kV) could be measured with a Trek electrostatic field probe. A modest voltage drift rate was observed in the sample voltage of <3 mV_s/sec. Without correction for drift, surface voltages can be measured for short periods of time—long enough for accurate surface sweeps—between recalibration of the probe. With a linear voltage drift correction, surface voltages can be measured to high accuracy for periods >4 hr between probe recalibration.

Data were acquired and processed using an automated Labview™ program. The SVP data are typically sampled at 1 kHz for 1 s intervals; averages and standard deviations are retained. Figure 6 shows a typical timing diagram for data acquisition. 10 s of data with the SVP positioned over a grounded plane are acquired before and after a 10 s interval of data acquired with the SVP positioned over the sample; V_{offset} and (V_{drifto}/τ_D) are determined through a linear fit to the grounded data, for offset and drift corrections using Eq. 2. For charge accumulation experiments, the SVP is then retracted, and the electron beam is un-blanked for different lengths of time from 10 s to 120 s. 1 s wait times were included after SVP movement to allow dissipation of electronic noise.

IV. THEORETICAL MODEL OF CHARGE ANS DISCHARGE

Theoretical models for sample charging and discharge are presented, based on dynamic bulk charge transport equations developed for electron charge carriers to predict the time, temperature, and electric field dependence of the sample net surface voltage. The model includes electron drift, diffusion, and displacement currents and makes direct ties to the interactions between injected electrons, which are trapped in localized states, and the magnitude and energy dependence of the density of those localized trap states within the gap; the carrier mobility, and the carrier trapping and de-trapping rates are then evaluated using the model.

V. TYPICAL MEAUREMENTS

Two types of measurements have been made on two prototypical polymeric spacecraft materials, LDPE and polyimide (Kapton HNTM) to illustrate the research capabilities of the new system [Hodges, thesis]. The polyimide sample was a 25 µm thick film of Kapton HN™ from Dupont. First, surface voltage measurements were made using a pulsed electron beam, while periodically measuring the surface voltage. Second, post charging measurements of the surface voltage were conducted, as deposited charge dissipated to a grounded substrate. This process allows for the collection of information about the material's electron yields and bulk resistivity. The good agreement is discussed between the fitting parameters of the model and the corresponding physical parameters determined from the literature and measurements by related techniques.

A. Charge Accumulation

Charge Accumulation

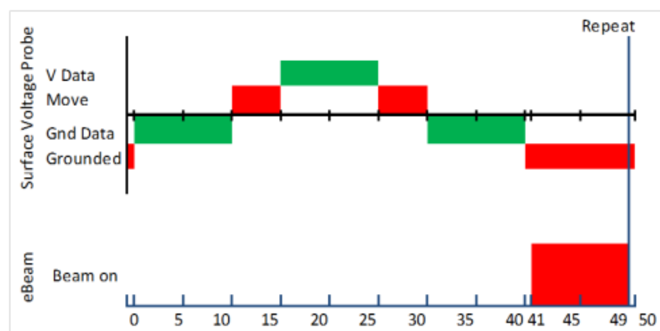

Fig. 6. Timing of a standard charge accumulation/ dissipation run. Green represents time at which data are being collected. Grounded times varied depending on the "beam on" time. For dissipation runs, the electron source was not used.

B. Charge Decay

Surface voltage profile measurements were made periodically during the electron beam charging process and as the polyimide sample discharged to a grounded substrate after exposure. The total dose of $9{\bullet}10^{-13}$ C (<1 pA-cm^{-2}) was delivered in approximately ten 5 µs pulses over ~30 min. The discharge curve is shown in Figure 4(b). An exponential decay with a time constant of τ_D=(16.7±0.8) hr provides a good fit to the long term data. Assuming that the charge all decays through ohmic conduction through the polyimide film to the grounded substrate, the resistivity of the polyimide $\rho=\tau_D/\varepsilon_o\varepsilon_r$ is ~$2{\bullet}10^{17}$ Ω-cm assuming a relative dielectric constant, ε_r, of 3.40. This is a factor of ~30 lower than the resistivity of Kapton measured by the charge storage method, $6{\bullet}10^{18}$ Ω-cm.[13]

Measurements are in progress to study voltage decay curves for additional materials, to determine dark current resistivities for various materials, and to study decays for longer periods of time. We are studying the voltage decay curves and their relation to determination of the "intrinsic" yields for highly insulating materials subject to charging by low-fluence probe beams.[7] We are also studying the initial rise in surface voltage often observed (see Figure 4(b)) to test its reproducibility and to determine if the effect is related to migration of internal charge layers or to post-irradiation electron emission.

C. Sweep

The spatial profile of the voltage across the sample surface, shown in Figure (a), was measured by sweeping the 7.0 mm diameter Au voltage sensor electrode (T) over a 10.0 mm diameter uniformly charged polyimide sample (E). The shape of the voltage profile is consistent with the convolution of a sensor disc with a uniformly charged sample disc. The spatial resolution for the larger diameter probe after deconvolution is estimated to be 1 mm to 2 mm. Preliminary measurements with the 3 mm diameter Au voltage sensor (U) indicate a better spatial resolution, on the order of 0.5 mm to 1 mm.

Measurements of the charge distribution on a polyimide sample from a focused, ~3 mm diameter electron beam demonstrated the capability of measuring nonuniform charge distributions on the sample. More such measurements are in progress, including ones to correlate the nonuniform charge distribution with a beam profile measured with a Faraday cup sensor and to monitor the lateral spread of the surface charge from a focused beam spot with time.

D. Charge Diffusion

Surface

ACKNOWLEDGEMENT

We gratefully acknowledge the fundamental inspiration, useful discussions, and encouragement of Robb Frederickson. Ryan Hoffmann and Neal Nickles were instrumental in developing the HGRFA and other aspects of the electron emission chamber. Prasanna Swaminathan helped in developing the use of the EFTP at USU.

REFERENCES

[1]J.R. Dennison, C.D. Thomson, J. Kite, V. Zavyalov, Jodie Corbridge, “Materials Characterization at Utah State University: Facilities and Knowledgebase of Electronic Properties of Materials Applicable to Spacecraft Charging,” *Proceedings of the 8th Spacecraft Charging Technology Conference*, Huntsville, Alabama, 2003.

[2]Neal Nickles, “The Role of Bandgap in the Secondary Electron Emission of Small Bandgap Semiconductors: Studies of Graphitic Carbon,” PhD Dissertation, Physics Dept,. Utah State University, 2002.

[3]W.Y. Chang, J.R. Dennison, Neal Nickles and R.E. Davies, “Utah State University Ground-based Test Facility for Study of Electronic Properties of Spacecraft Materials,” *Proceedings of the 6th Spacecraft Charging Technology Conference*, Air Force Research Laboratory Science Center, Hanscom Air Force Base, MA, 1999.

[4]*C.D. Thomson, V. Zavyalov, J.R. Dennison, “Instrumentation for studies of electron emission and charging from insulators,” Proc. of 8th Spacecraft Charging Technology. Conf., Huntsville, Alabama, 2003.*

[5]C.D. Thomson, “Measurements of the Secondary Electron Emission Properties of Insulators”, Ph.D. Dissertation, Physics Dept., Utah State Univ., 2004.

[6]J.R. Dennison, Alec Sim and Clint Thomson, “Evolution of the Electron Yield Curves of Insulators as a Function of Impinging Electron Fluence and Energy,” *IEEE Transaction on Plasma Science,* Vol. 34, No. 5, October 2006, pp. 2204-2218.

[7]Ryan Hoffmann, JR Dennison Clint D. Thomson and Jennifer Albresten, “Low-fluence Electron Yields of Highly Insulating Materials” *IEEE Transaction on Plasma Science,* Vol. 36, No. 5, October 2008, pp. 2238-2245.

[8]I. Krainsky, W. Lundin, W.L. Gordon, and R.W. Hoffman, Secondary Electron Emission Yield Annual Report for Period July 1, 1979 to June 30, 1980, Case Western Reserve University, Cleveland, OH, 1980 (unpub.).

[9]Prasanna Swaminathan , “Measurement of Charge Storage Decay Time and Resistivty of Spacecraft Insulators,” MS Thesis, Electrical and Computer Engineering Department; Utah State University, 2004.

[10]Prasanna Swaminathan, A. R. Fredericksn, J.R. Dennison, Alec Sim, Jerilyn Brunson, Eric Crapo· “Comparison Of Classical And Charge Storage Methods For Determining Conductivity Of Thin Film Insulators,” *Proc. of 8th Spacecraft Charging Technology Conf.*, , Huntsville, Alabama, October 20-24, 2003.

[11] A.R. Frederickson and J.R. Dennison, “Measurement of Conductivity and Charge Storage in Insulators Related to Spacecraft Charging,” *IEEE Transaction on Nuclear Science*, Vol. 50, No. 6, December 2003, pp. 2284-2291.

[12]not used

[13]A.R. Frederickson, C. E. Benson and J. F. Bockman, “Measurement of Charge Storage and Leakage in Polyimides,” *Nuclear Instruments and Methods in Physics Research B*, 454-60, 2003.

[14]L. Levy, D. Sarrail, and J. M. Siguier, “Conductivity and secondary electron emission properties of dielectrics as required by NASCAP,” *Third European Symposium on Spacecraft Materials in Space Environment*, 1993, pp. 113-123.

[15]R. Coelho, L. Levy, and D. Sarrail, “Charge decay measurements and injection in insulators,” *Journal of Applied Physics*, Vol. 22, No. 9, Sept. 1989, pp. 1406-1409.

A. D. Hastings, and H. Garrett, *Spacecraft-environment Interactions*, Cambridge University Press, 1996.

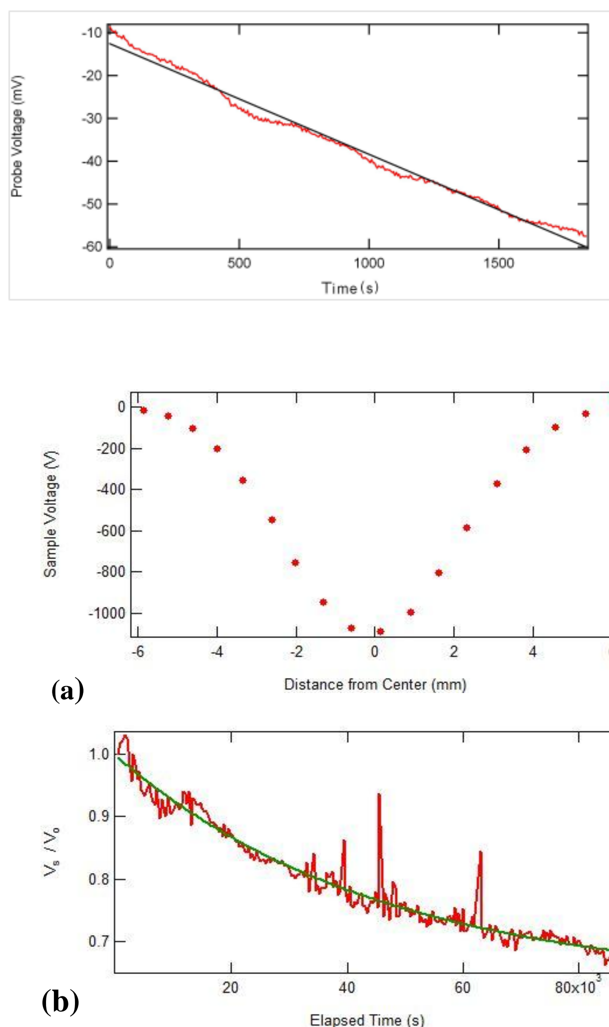

Fig. 7. Flipper measurements. *(a) Sweep of 7.0 mm diameter Au voltage sensor electrode over a 10.0 mm diameter uniformly charged polyimide sample. (b) Temporal decay of normalized surface voltage of a charged polyimide sample. The fit is an exponential decay with a time constant of* $(6.0\pm0.3)\cdot10^3$ *s.*

B Frederickson, A.,A. Whittlesey and H. Garrett, 2001, "Comparing CRRES Internal Discharge Monitor Results with Ground Tests and Published Guidelines," Spacecraft Charging Technology.

C. D. Ferguson, "New Frontiers in Spacecraft Charging," *IEEE Trans. Plasma Sci.*, vol. 40, no. 2, pp. 1-5, Feb. 2012.

D J.R. Dennison, Prasanna Swaminathan, Randy Jost, Jerilyn Brunson, Nelson Green and A. Robb Frederickson, "Proposed Modifications to Engineering Design Guidelines Related to Resistivity Measurements and Spacecraft Charging," *Proceedings of the 9th Spacecraft Charging Technology Conference,* (Epochal Tsukuba, Tsukuba, Japan, April 4-8, 2005).

E ASTM D 257-99, Standard Test Methods for DC Resistance or Conductance of Insulating Materials, (1999).

F Jerilyn Brunson, "Measurement of Charge Decay Time and Resistivity of Spacecraft Insulators Using Charge Storage Method and Application to Theoretical Modeling of Charging Behavior of Insulators," PhD Dissertation; Physics Department; Utah State University, 2009.

G Alec M. Sim and JR Dennison, "Unified Density of States Based Model of Electron Transport and Emission of Spacecraft Materials," *Proceedings of the* 12*th Spacecraft Charging Technology Conference,* (Kitakyushu, Japan, May 14-18, 2012), in preparation.

H Joshua L. Hodges, "*In Situ* Measurements of Electron Beam Induced Surface Voltage of Highly Resistive Materials," MS Thesis, Physics Department; Utah State University,2012.

I. Frooninckx, T. B., and J. J. Sojka (1992), Solar Cycle Dependence of Spacecraft Charging in Low Earth Orbit, J. Geophys. Res., 97(A3), 2985–2996.

J Gregory Wilson and JR Dennison, "Approximation of Range in Materials as a Function of Incident Electron Energy," *IEEE Trans. on Plasma Sci.*, **40**(2), 305-310 (2012).

K NASA Technical Handbook, "Mitigating In-Space Charging Effects —A Guideline," NASA-STD-4002A, 2011.

L Justin Dekany, Robert H. Johnson, Gregory Wilson, Amberly Evans and JR Dennison, "Ultrahigh Vacuum Cryostat System for Extended Low Temperature Space Environment Testing," *Proceedings of the* 12*th Spacecraft Charging Technology Conference,* (Kitakyushu, Japan, May 14-18, 2012)

M Robert Davies, "Measurement of Angle-resolved Secondary Electron Spectra," PhD Dissertation, Physics Department; Utah State University, 1999.

N Jason Kite, "Secondary Electron Production and Transport Mechanisms by Measurement of Angle-Energy Resolved Cross Sections of Secondary and Backscattered Electron Emission," PhD Dissertation; Physics Department; Utah State University, 2007.

O Clint Thomson, "Measurements of the Secondary Electron Emission Properties of Insulators," PhD Dissertation; Physics Department; Utah State University, 2004.

P L. Malter, "Anomalous Secondary Electron Emission A New Phenomenon." *Phys. Rev*.,49, 478.1936.